UACJ Technical Reports, Vol.5 (2018), pp. 32-44

論　文

Strain Rate Dependence of the Material Strength in 5xxx Series Aluminum Alloys and the Evaluation of Their Constitutive Equation*

Hiroyuki Yamada**, Tsuyoshi Kami***, Ryota Mori****
Tomoyuki Kudo*****, and Minemitsu Okada******

The effect of strain rate on the mechanical properties of 5xxx series aluminum alloys containing solute Mg atoms (5005, 5021, 5082 and 5182) and pure aluminum (1070) was investigated within a wide strain rate range of 1.0×10^{-4} to 1.0×10^{3} s^{-1} at room temperature. The 1070 exhibited a positive strain rate dependence of material strength at the investigated strain rates. However, the 5xxx series aluminum alloys primarily exhibited the negative strain rate dependence of material strength and serration caused by the Portevin-Le Chatelier effect on the Mg content and strain rate. As a result of using the material constitutive equation for the negative strain rate dependence, it was found that the flow stress may change in the dynamic strain rate range. However, it was found that the strain rate dependence of material strength differed in the 5082 and the 5182 alloys. It would be caused by less solute Mg of the Al phase in the 5182 alloy than in the 5082 alloy, because more Mg_2Si compounds precipitated on Mn bearing particles as precipitation sites in the 5182 alloy.

Keywords: *serration; strain rate; dynamic; impact; constitutive equation; Al-Mg alloy; pure aluminum;*

1. Introduction

Many constitutive equations have been proposed for the strain rate and temperature effect [1]. In these equations, the flow stress is expressed as a function of various parameters, as follows:

$$\sigma = f(\varepsilon, n, Y, \dot{\varepsilon}, T) \quad (1)$$

where ε is the strain, n is the work hardening rate, Y is the yield stress, $\dot{\varepsilon}$ is the strain rate, and T is the testing temperature. Therefore, it is necessary to conduct experiments within a wide strain rate range and testing temperature. Typically, experiments have been conducted by using a universal testing machine for the quasi-static strain rate in the range of 10^{-5} to 10^{-1} s^{-1}, and the Split Hopkinson Pressure (SHB) method [2, 3] for the high strain rate. The SHB method applies the one-dimensional elastic wave propagation theory, which has become the commonly accepted test method for the impact strain rates in the range of 10^{2} to 10^{4} s^{-1}. However, material properties at the dynamic strain rate in the range of 10^{0} to 10^{1} s^{-1} have barely been investigated because it is difficult to measure the dynamic tests in principle by using the SHB method. In the dynamic strain rate range, it is known that the flow stress starts to increase rapidly. Thus, the material properties at those strain rates are important.

The 5xxx series aluminum alloys containing solute Mg atoms (Al-Mg alloys) can be cited as an example of materials that exhibit various strain rate sensitivity. The Al-Mg alloy has been tested at various strain rates and testing temperatures because it exhibits high strength and corrosion resistance. Tests with the Al-Mg alloy have shown that the serrated flow stress occurs frequently in a stress-strain curve called "serration". This happens because the solute Mg atoms interact with the dislocations [4)~8)].

* The main part of this paper has been published in Metals **8** (2018), 576.
** Department of Mechanical Engineering, National Defense Academy
*** Graduate School of Science and Engineering, National Defense Academy
**** Development Department Ⅰ, Research and Development Division, UACJ Corporation
***** Development Department Ⅰ, Research and Development Division, UACJ Corporation
****** No.1 Product Design Section, Quality Assurance Department, UACJ (Thailand) Co., Ltd.

This phenomenon is known as the Portevin-Le Chatelier (PLC) effect and depends on the strain rate and temperature [9]. This serration phenomenon has been reported for various metallic materials besides aluminum alloys [10)~13)]. When serration occurs, a pattern may be formed on the material surface. For this reason, it is desirable to suppress the serration industrially, and many previous studies have investigated the serration occurrence conditions [14), 15)].

Previous studies have reported that a negative strain rate dependence of the material strength has been observed for Al-Mg alloys at a quasi-static strain rate [4), 14), 15)]. In contrast, a positive strain rate dependence of material strength has been confirmed for a high strain rate [15), 16)]. This results from the effect of the solute Mg atoms, which can effectively lock the dislocation at a low strain rate and moderate the temperature (e.g., room temperature). However, the interaction between the Mg atoms and the dislocations decreases as the strain rate increases [15), 16)].

The strain rate at which the strain rate dependence shifts from negative to positive has not yet been clarified [4), 15)]. For example, the boundary of the strain rate at which the negative strain rate dependence of the 5182 aluminum alloy (containing 4.5 wt.% Mg) is not observed at room temperature has been proposed as the dynamic strain rate of 10^0 s^{-1} [15)]. Therefore, it is important to determine the material properties of the Al-Mg alloys at the dynamic strain rate. Additionally, there exist few studies on the influence of the dynamic strain rate on the 5xxx series aluminum alloys with different amounts of Mg content.

In this study, in order to clarify the strain rate dependence of the serration behavior of Al-Mg alloys, tensile tests were conducted at room temperature and within a wide strain rate range, including the dynamic range. We also attempted to apply the constitutive equation to the material, including the strain rate effect.

2. Materials and Methods

2.1 Specimen

In this study, various 5xxx series aluminum alloys, namely, 5005, 5021, 5082, and 5182 aluminum alloys, with different amounts of Mg content were selected and will be hereinafter referred to as the 5005 alloy, 5021 alloy, 5082 alloy, and 5182 alloy, respectively. In comparison with the 5082 and 5182 alloys, the Mg content amount was almost the same; however, the amount of the Mn content was different. In comparison with these Al-Mg alloys, commercial pure aluminum, namely, 1070 pure aluminum was also prepared. The chemical compositions and the average grain size of the investigated alloys are listed in **Table 1**.

The specimen geometry is shown in **Fig. 1**. All specimens were machined from rolled materials using a lathe. The gauge length of the specimen was 8 mm and its diameter was 5 mm. All of the specimens were annealed at 618 K in air. The annealing time was 3.6 ks for 1070 and 7.2 ks for the Al-Mg alloys, respectively. Subsequently, the specimens were furnace cooled to room temperature. Tensile tests were conducted three times for each strain rate using these specimens.

2.2 Tensile Test

2.2.1 Quasi-Static Test

Quasi-static tensile tests were performed at room temperature by using a universal testing machine (Instron, 5500R, USA). The initial strain rates ($\dot{\varepsilon} = V/$

Table 1 Chemical compositions and the average grain size of the investigated alloys (mass. %).

Alloy	Si	Fe	Cu	Mn	Mg	Cr	Zn	Ti	Al	Grain Size (μm)
1070	0.04	0.18	0.00	0.00	0.00	0.00	0.00	0.01	99.77	26
5005	0.16	0.29	0.03	0.02	0.76	0.00	0.01	0.01	Bal.	99
5021	0.13	0.27	0.07	0.25	2.28	0.03	0.03	0.03	Bal.	54
5082	0.11	0.20	0.03	0.14	4.50	0.06	0.02	0.01	Bal.	32
5182	0.09	0.20	0.05	0.34	4.40	0.02	0.03	0.02	Bal.	29

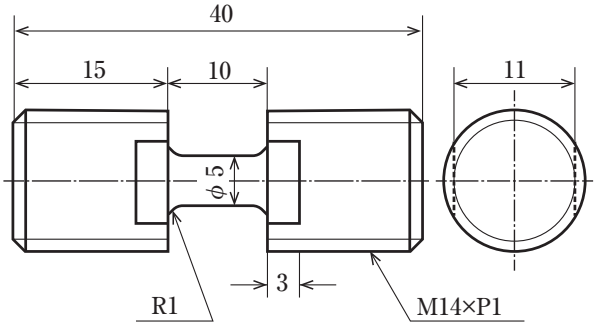

Fig. 1 Specimen geometry (mm).

L: V is the crosshead speed and L is the gauge length) were chosen in the range of 1.0×10^{-4} to 1.0×10^{-1} s^{-1}.

2.2.2 Dynamic Test

A dynamic tensile test [17] was conducted at room temperature by using the servo-hydraulic testing machine (Institute of Space Dynamics, HVUT-H-10T, Japan). The configuration of the testing apparatus is shown in **Fig. 2**. The capacity of the load cell, which was developed by our laboratory, was located at the end of the fixed rod and amounted to 10 kN. The displacement of the specimen was measured by using a laser displacement sensor (KEYENCE, LK-H155, Japan). The sampling rate was 100 kHz.

First, to stabilize the flow of the hydraulic system, the piston moved downward without the load. Then, since the piston pulled the moving rod, the tensile load was applied to the specimen. Additionally, the displacement increased with the plastic deformation of the specimen. The specimen deformation was calculated by subtracting the outputs of two displacement sensors (sensor ① and ②). Because the pressure of the servo-hydraulic system increased slightly during the test, the strain rate also increased. The average strain rate during the test was calculated.

2.2.3 Impact Test

The SHB method [2, 3] was used in the impact tensile test. **Fig. 3** shows the configuration of the SHB apparatus (Institute of Space Dynamics, ST-R-5000,

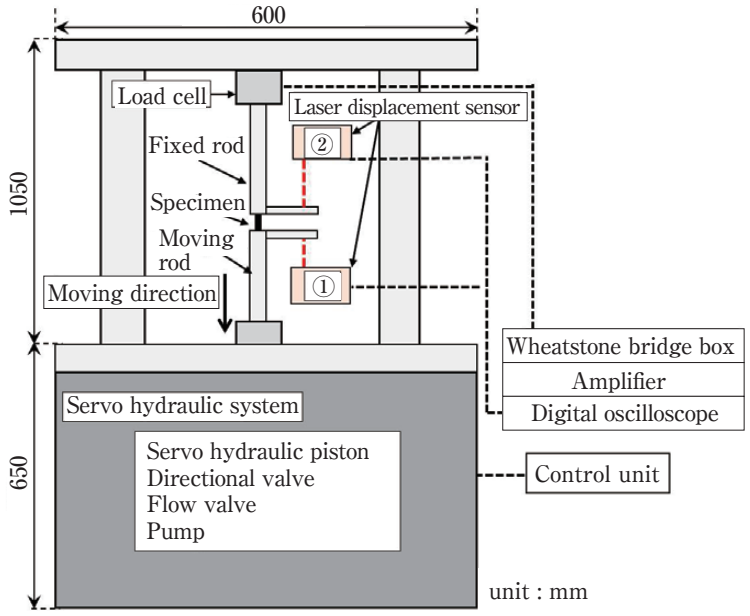

Fig. 2 Configuration of the servo-hydraulic testing apparatus [17].

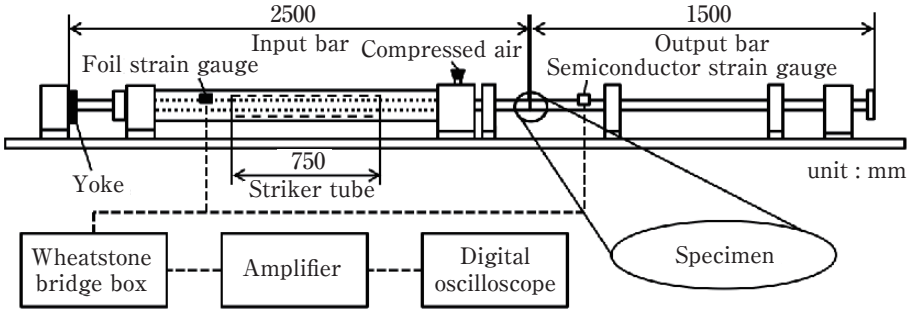

Fig. 3 Configuration of the split Hopkinson pressure (SHB) apparatus [18].

Japan)[18]. The main components of this apparatus are the striker, input bar, and output bar. After the striker impacts the yoke, the tensile stress wave propagates through the input bar. When the wave reaches the specimen, part of it propagates through the output bar and the remaining part is reflected on the specimen. These waves were measured by using a foil strain gauge (KYOWA, KFG-2-120-C1-16, Japan) and semiconductor strain gauge (KYOWA, KSP-1-350-E4, Japan), which attached to the input and output bars, respectively. The sampling rate was 1 MHz.

By applying the one-dimensional elastic wave propagation theory, we were able to derive the nominal stress ($\sigma(t)$), nominal strain ($\varepsilon(t)$), and strain rate ($\dot{\varepsilon}(t)$) in the specimen, as follows:

$$\sigma(t)=\frac{AE}{A_S}\varepsilon_t(t) \tag{2}$$

$$\varepsilon(t)=\frac{2c_0}{l_S}\int_0^t[\varepsilon_i(t)-\varepsilon_t(t)]\,dt \tag{3}$$

$$\dot{\varepsilon}(t)=\frac{2c_0}{l_S}[\varepsilon_i(t)-\varepsilon_t(t)] \tag{4}$$

where A_s is the cross-sectional area of the specimen; A and E are the cross sectional area and Young's modulus of the input and output bars, respectively; c_0 is the velocity of the elastic wave; l_s is the gauge length of the specimen; $\varepsilon_i(t)$ and $\varepsilon_t(t)$ are the incident and transmitted waves, respectively. The average strain rate during the test was calculated by Equation (4).

3. Results

The stress–strain relationship of the 1070 is shown in **Fig. 4**. The flow stress increased significantly with the strain rate. It can be said that the 1070 exhibited a positive strain rate dependence, which is common behavior for 1100[19), 20)].

Fig. 5a–d shows the stress–strain relationship of the 5xxx series aluminum alloys and these enlarged views. In the 5005 alloy, a positive strain rate dependence was observed. However, in the 5021 alloy, which had a larger amount of Mg in comparison with the 5005 alloy, the serration behavior could be confirmed in the strain rate range of 10^{-4} to 10^{-2} s^{-1}. Additionally, the negative strain rate dependence could be confirmed. However, the flow stress at the impact strain rate (7.9×10^{2} s^{-1}) increased in comparison with the results obtained by the quasi-static test. In contrast, in the 5082 and 5182 alloys, the negative strain rate dependence was strong because the added Mg amount was large and induced serration in the quasi-static strain rate range of 10^{-4} to 10^{-1} s^{-1}. For the 5182 alloy, the flow stress increased slightly from the strain rate of 10^{-1} s^{-1} to the impact strain rate. This result was different from the result obtained with the 5082 alloy, which contained almost the same amount of Mg.

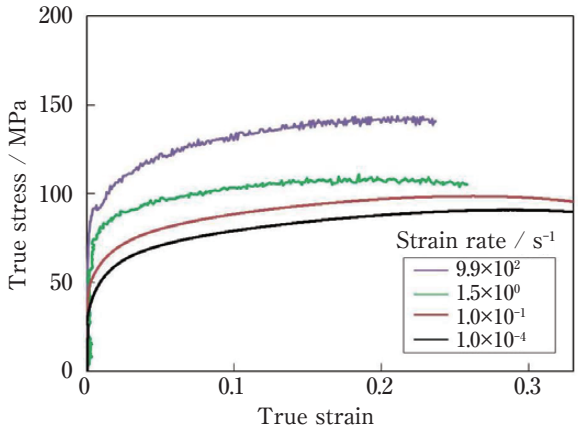

Fig. 4 Stress–strain relationship of 1070.

4. Discussion

4.1 Previous Studies on Serration Theory[17)]

In previous studies, the following mechanism of serration occurrence was proposed[21), 22)]. First, the movement of the dislocations is prevented by short-range obstacles such as the forest dislocation and solute atom. Secondly, the dislocations are temporarily arrested for a certain amount of time, which is defined as the waiting time t_w. Finally, the dislocations overcome the obstacles and move to other obstacles. These processes are repeated and the movement of dislocation is discontinuous owing to interaction with the solute Mg atoms.

During the waiting time (t_w), the solute Mg atoms can move to the dislocations and temporarily lock

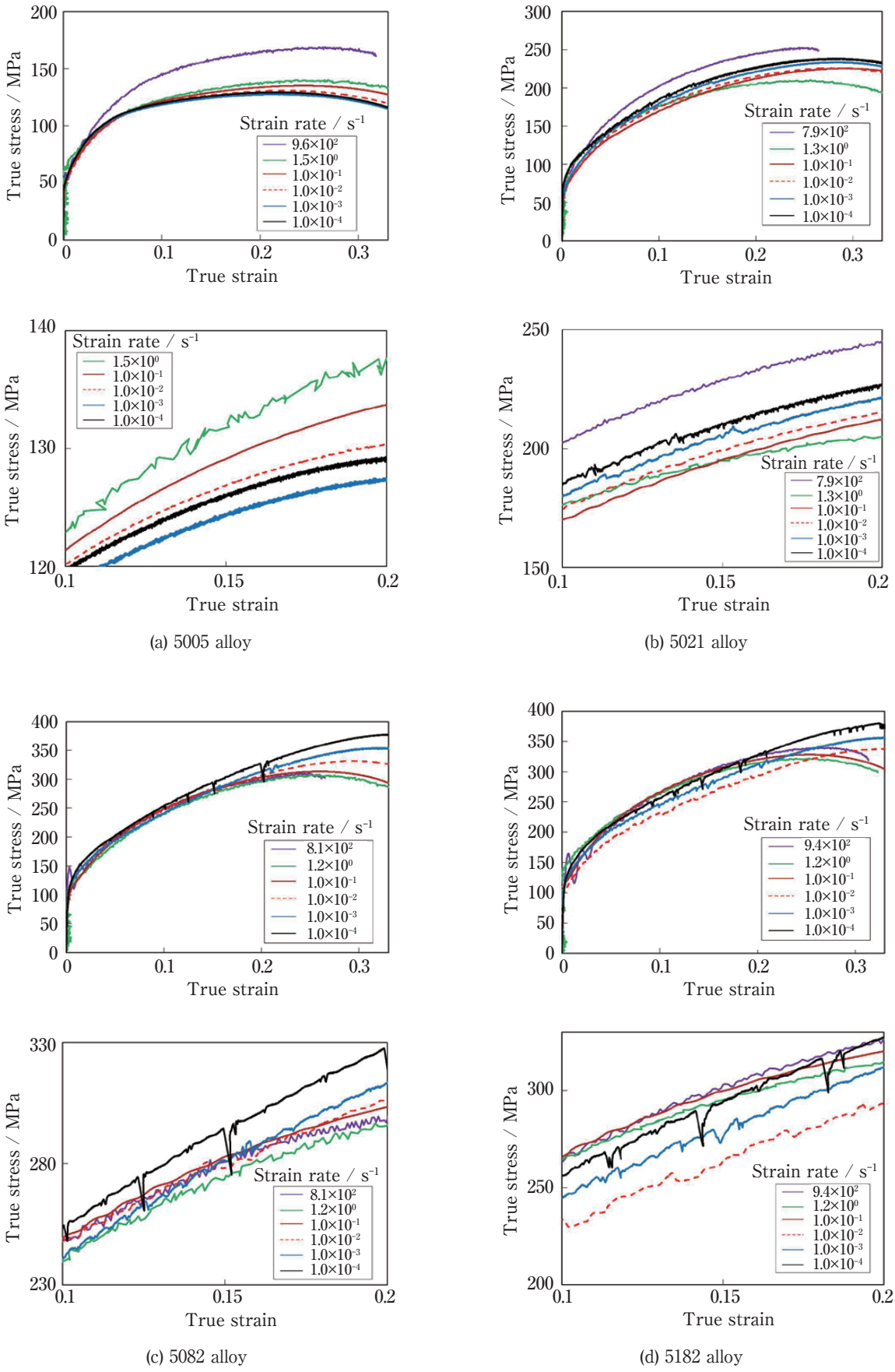

(a) 5005 alloy

(b) 5021 alloy

(c) 5082 alloy

(d) 5182 alloy

Fig. 5 Stress–strain relationship of (a) 5005 alloy, (b) 5021 alloy, (c) 5082 alloy, and (d) 5182 alloy and these enlarged views.

them. The waiting time is related to the strain rate as follows [21), 22)] :

$$t_w = \frac{\rho b L}{\dot{\varepsilon}} \quad (5)$$

where ρ is the dislocation density, b is the Burgers vector, and L is the average distance between the obstacles. If the dislocations are sufficiently locked by the solute Mg atoms, the serrations will start to appear [21)]. The condition necessary for the appearance of serration can be expressed as follows [21), 23)] :

$$t_w \geq t_a \quad (6)$$

where t_a is the time required for the solute Mg atoms to fully lock the dislocations. It can be said that the smooth flow stress is observed if t_w is less than t_a [21)]. Additionally, a previous study suggested that a negative strain rate dependence is closely related to the occurrence of serration [4)].

4.2 Effect of Strain Rate on Serration Behavior

Here, we discuss the results obtained with the 5xxx series alloys in which serration occurred. From Equation (5), it can be said that t_w is sufficiently larger than t_a at low strain rate. This resulted in the negative strain rate dependence at low strain rates owing to the Mg atoms-dislocation interaction. In such cases, a large force is required to break the atmosphere of the Mg atoms. As the strain rate increased ($t_w < t_a$), the solute Mg atoms-dislocation interaction decreased [21)]. In fact, a smooth stress–strain curve was observed over the dynamic strain rate. It is known that the deformation of metals at a high strain rate can be understood by the thermal activation theory of dislocation motion [24)]. According to this theory, overcoming short-range obstacles depends on the strain rate value. The deformation of pure aluminum is governed by this theory [20)], and can also be inferred from Fig. 4. For example, in the 5021 alloy, at high strain rate, the flow stress increased at strain rates from 1.0×10^0 to 7.9×10^2 s^{-1}. This suggests that the deformation mechanism of the 5021 alloy at these strain rates was similar to the deformation mechanism of 1070. At high strain rate, the thermal activation theory became the dominant mechanism because the Mg atoms could not migrate to the dislocation at such high strain rate. The effect of the strain rate in other alloys will be discussed in detail in the next section.

As mentioned above, the effect of the solute Mg atoms depends on the strain rate. This exerts a significant effect on the mechanical properties of the Al-Mg alloy. To determine the dependence of the material strength on strain rate, it is important to obtain the material properties within a wide strain rate range. In particular, the dynamic strain rate range from 10^0 to 10^1 s^{-1} is very important because the strain rate dependence of this alloy changes at those strain rates and significantly affects the development of the constitutive equation.

4.3 Positive Strain Rate of Flow Stress

The relationship between the flow stress and the strain rate of materials with a positive strain rate dependence is often used in the Johnson–Cook equation [25)]. In this study, we attempted to fit the Johnson–Cook expression to the experimental results obtained with 1070. However the error in the experimental results was large. A previous study has reported that the relationship between the strain rate and the flow stress could not be expressed by the Johnson–Cook equation [1), 19)]. For example, it is known that the flow stress of pure aluminum, such as the 1070 used in this study, exhibits an exponential curve as the strain rate increases [19)]. For this reason, to improve the Johnson–Cook equation, Khan et al. proposed the following expression [15), 19)] :

$$\sigma = \left[A + B\varepsilon^{n_0}\left(1 - \frac{\ln\dot{\varepsilon}}{\ln D}\right)^{n_1}\right]\left(\frac{\dot{\varepsilon}}{\dot{\varepsilon}_{ref}}\right)^{C} T^{*m} \quad (7)$$

where σ is the flow stress, ε is the plastic strain, $\dot{\varepsilon}$ is the strain rate, $\dot{\varepsilon}_{ref}$ is the reference strain rate, and T^* is the normalized temperature $T^* = (T_m - T)/(T_m - T_r)$, where T_m is the melting point temperature, T is the testing temperature, and T_r is the reference temperature. A, B, n_0, D, n_1, C, and m are material constants, and D is considered as 10^6 s^{-1}. In this study, for testing at room temperature, $T = T_r$. Thus, T^* was not considered. Additionally, $\dot{\varepsilon}_{ref}$ was set to 10^{-4} s^{-1}, which was the slowest strain rate in this experiment.

Table 2 summarizes the material constants that

were determined to minimize the error between Equation (7) and the experimental result obtained with 1070. **Fig. 6** shows the relationship between the flow stress and the strain rate at the true strains of 0.05, 0.1, and 0.2 in the 1070. The curve obtained from Equation (7) is also shown in Fig. 6. The increase in the flow stress as the strain rate increased had a tendency that was similar to the relationship between the flow stress and the strain rate of the 1100 aluminum [23].

4.4 Negative Strain Rate of Flow Stress

There are few material constitutive equations that express a negative strain rate dependence. It is known that the negative strain rate dependence is closely related to the occurrence of serrations and greatly affected by the temperature and strain rate. This is because the pinning of dislocation largely depends on the diffusion rate of the Mg atoms and the movement rate of dislocation.

Many discussions have been conducted with regard to the temperature and strain rate conditions required for the serration to occur. In a previous study, it was reported that serration occurred in a 5182 alloy when the testing temperature was between 193 K and 383 K and the strain rate was 10^{-1} s^{-1} or less. Kabrian et al. [15] investigated the strain rate dependence of the 5182 alloy and found that a negative strain rate dependence occurred under a temperature between 296 K and 373 K and strain rate of 10^{0} s^{-1} or less. Therefore, they suggested the constituent rule expressed by the following equation:

$$\sigma=\left[A+B\varepsilon^{n_0}\left(1-\frac{\ln\dot{\varepsilon}}{\ln D}\right)^{n_1}T^{*m_1}\right]\left\{(\exp(K_1\dot{\varepsilon})-\left[C_1\exp(-K_2\dot{\varepsilon})\left(\frac{T}{T_m}\right)^{m_2}\left(\frac{\varphi}{1+|\varphi|}\right)\right]\right\}T^{*m_3} \quad (8)$$

where m_1, K_1, C_1, K_2, m_2, and m_3 are constants. The other constants were the same as those in Equation (7). φ is a value representing the temperature dependence of serration occurrence and is defined by the following equation:

$$\varphi=\frac{T-T_C}{T_C} \quad (9)$$

where, T_C is the boundary temperature where the strain rate dependence changes from negative to positive. Kabrian et al. [15] set T_C to 373 K, and the same value was used in this study.

4.4.1 Effect of Mg Content

The material constants of the 5xxx series aluminum alloys were determined by changing the constants of Equation (8) and are summarized in **Table 3**. The relationship between the flow stress and the strain rate of the 5021 and 5082 alloys indicated a typical behavior, as shown in **Fig. 7**. The curves obtained from Equation (8) are also shown in this figure. The change of the flow stress with the increasing strain rate roughly agreed with the model shown in Equation (8). For both the 5021 and 5082 alloys, it was possible to confirm a negative strain rate dependence up to the strain rate of approximately 10^{0} s^{-1}.

Table 2 Parameter values of 1070 aluminum for Equation (7).

A	B	n_0	n_1	C
33	97	0.185	-0.64	0

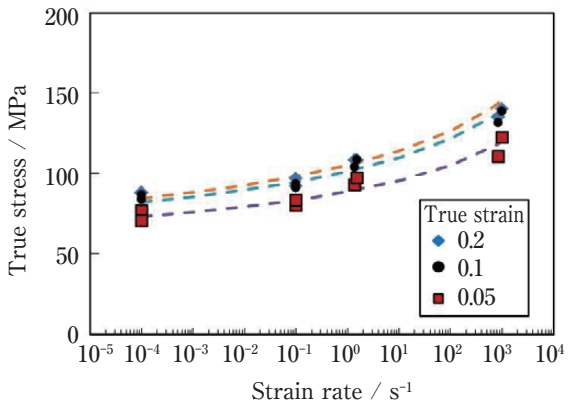

Fig. 6 Stress and strain rate relationship of 1070 aluminum. The curves indicated by broken line were obtained from Equation (7).

Table 3 Obtained parameters of Equation (8) in 5xxx series aluminum alloys.

Alloy	A	B	n_0	n_1	K_1	C_1	K_2	m_2
5005	23.11	154.70	0.20	-0.07	0.00016	0.00	0.00	0.00
5021	25.41	359.60	0.38	0.02	0.00016	1.06	693.62	1.09
5082	78.00	507.13	0.50	0.00009	0.00001	59.6	1358.60	4.38
5182	79.90	485.88	0.50	0.00	0.00013	1.03	599.89	0.28

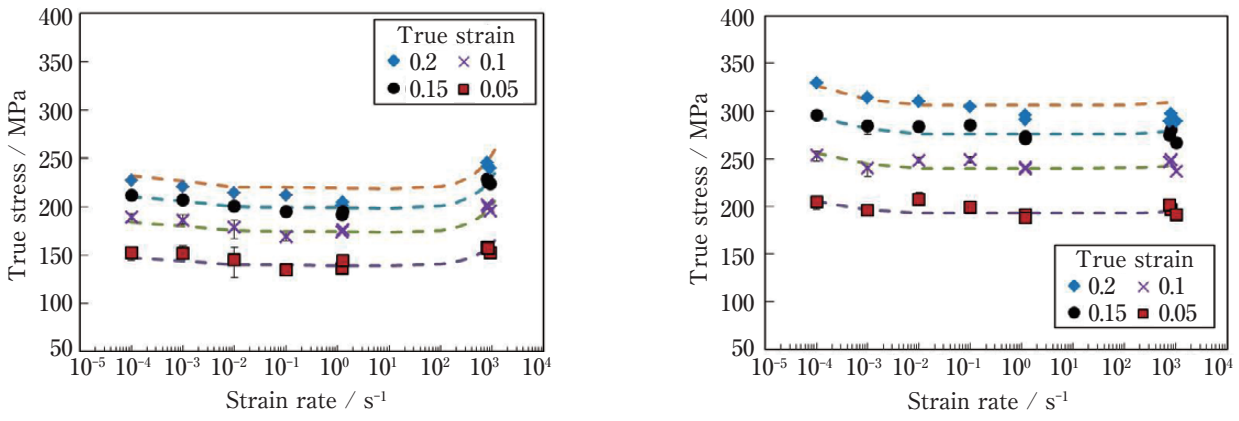

(a) 5021 alloy (b) 5082 alloy

Fig. 7 Stress and strain rate relationship of (a) 5021 and (b) 5082 aluminum alloys. Curves indicated by dashed lines were obtained from Equation (8).

Fig. 8 summarizes the relationship between the flow stress and the strain rate at the true strain of 0.2 in the investigated pure aluminum and aluminum alloys. As the amount of Mg increased, the strength increased by the solid solution hardening, while the negative strain rate dependence increased at a low strain rate. This occurred because the deformation resistance inside the material increased by the pinning of dislocation as a result of the Mg solution, which was strongly affected by the large amount of Mg content and the low strain rate, as mentioned above. The effect of the solid solution hardening caused by the Mg content was confirmed even with the 5005 alloy, whose Mg content was smaller than that of other alloys. However, the pinning effect of the dislocation was weak since the amount of Mg addition was small. Therefore, it was assumed that the positive strain rate dependence was confirmed, because in the 5005 alloy with a small amount of Mg content, the chemical composition tended towards that of pure aluminum. However, the positive strain rate dependence was smaller than that of 1070, since the 5005 alloy had more obstacles preventing the dislocation movement, as compared with 1070.

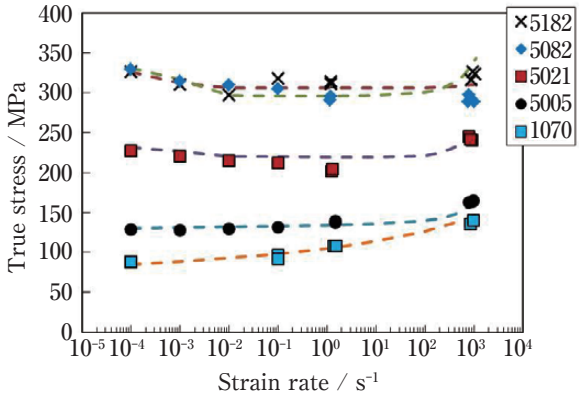

Fig. 8 Relationship between the flow stress and the strain rate at the true strain of 0.2 in the investigated pure aluminum and the aluminum alloys.

4.4.2 Effect of Mn Content

In the 5182 alloy, the flow stress decreased monotonically as the strain rate increased from 1×10^{-4} to 1×10^{-2} s^{-1}. However, the flow stress increased when the strain rate increased from 1×10^{-1} s^{-1} to approximately 1×10^{3} s^{-1} in comparison with above strain rate range. This behavior was similar to the relationship between the strain rate and the flow stress of the same alloy, which has been reported by a previous study [26]. However, it was different from the behavior of the 5082 alloy, which contained almost the same Mg amount. Because the average grain sizes of the 5082 and 5182 alloys were 32 and 29 μm, respectively, as shown in Table 1, it was considered that their influence was negligible. Thus, the effect of additives was considered because both alloys differed in the amount of Mn content.

Essentially, the Mn element behaves as a solid solution, similar to the Mg element in an aluminum alloy. However, it has been reported that some Mn elements produce the dispersive phases of Al_6Mn

(intermetallic compound) [27]. Therefore, to confirm the influence of the microstructure by the added Mn content, the observation of the dispersive phase in the 5082 and 5182 alloys was attempted by using a Transmission Electron Microscope (TEM). The thin film for the TEM was prepared by electro-polishing. Constituted elements of the particles observed in TEM images were also analyzed by Energy Dispersive Spectroscopy (EDS). **Fig. 9** shows the bright-field TEM images of the 5082 and the 5182 alloys. According to TEM observation, microstructures were significantly different between the 5082 and the 5182 alloys. Comparatively coarse particles and fine particles were observed in the 5082 alloy. In contrast, spherical particles and needle-like particles adjacent to the spherical particles were observed in the 5182 alloy, and both particles size was as large as the coarse particles in 5082 alloy. By EDS analysis (**Fig. 10**), the coarse particles in the 5082 alloy were Mg_2Si compound and fine particles were Al-Mn-Fe or Al-Cr compound. In the 5182 alloy, spherical and needle-like particles were Al-Mn-Fe-Si compound and Mg_2Si compound, respectively. Number densities of particles in the 5082 and the 5182 alloys were 2.9/μm^3 and 4.9 /μm^3, respectively.

As the solute Mg of Al phase increased, the negative strain rate dependence expanded to a high strain rate because of the Portevin-Le Chatelier (PLC) effect. The 5082 and the 5182 alloys homogenization treatment carried out at around 773 K for 21.6 ks after casting. In

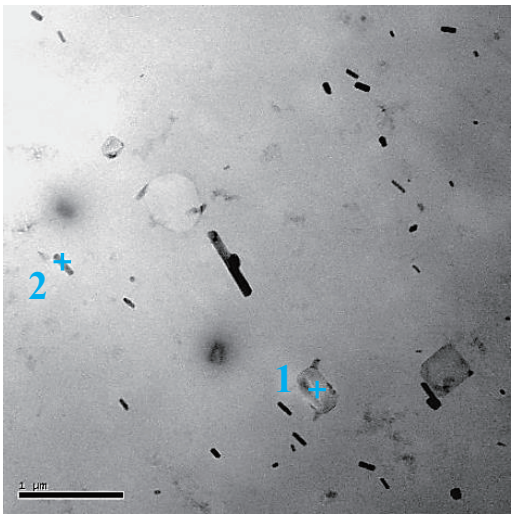

(a) 5082 alloy field 1

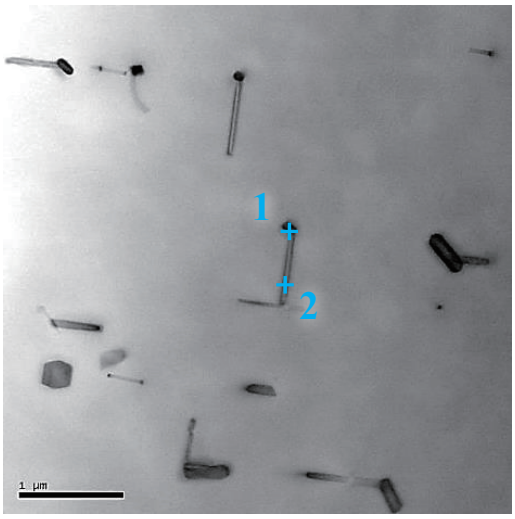

(c) 5182 alloy field 1

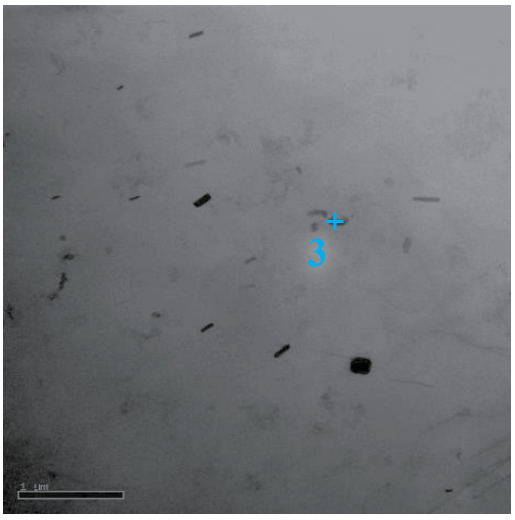

(b) 5082 alloy field 2

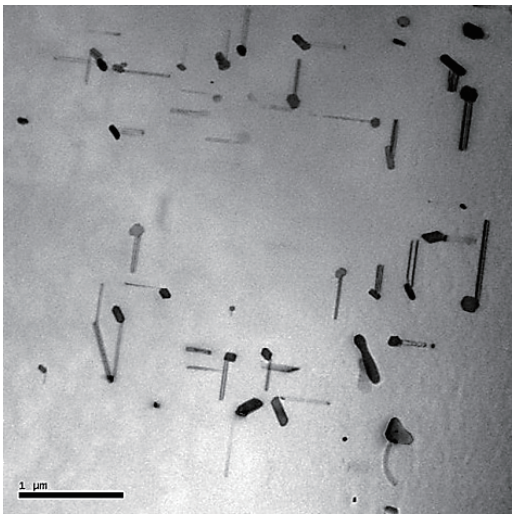

(d) 5182 alloy field 2

Fig. 9 TEM images of 5082 and 5182 alloys. (a) 5082 alloy field 1, (b) 5082 alloy field 2, (c) 5182 alloy field 1, (d) 5182 alloy field 2.

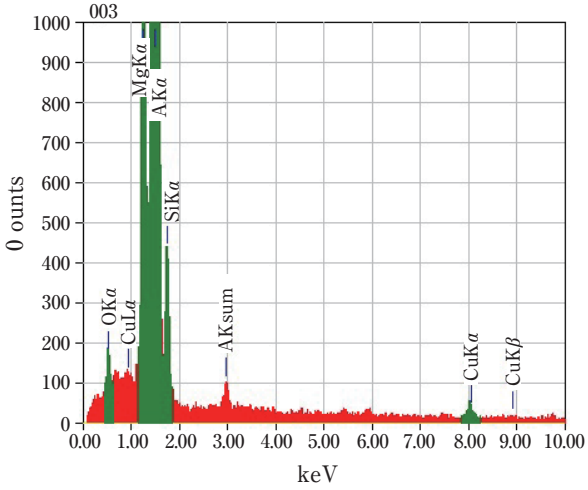

(a) Coarse particle 1 (Mg_2Si)
5082 alloy

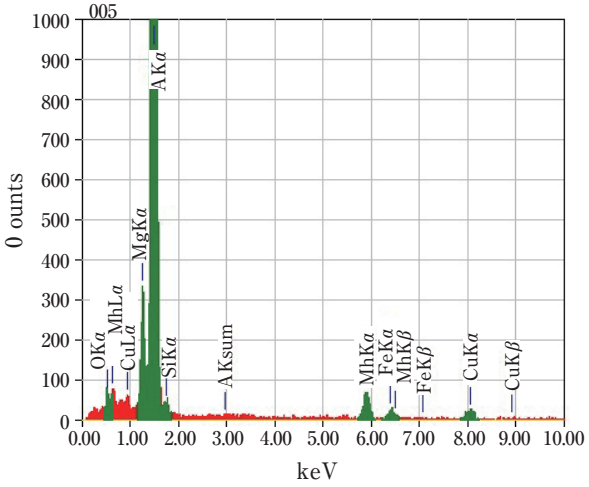

(d) Spherical particle 1 (Al-Mn-Fe compound)
5182 alloy

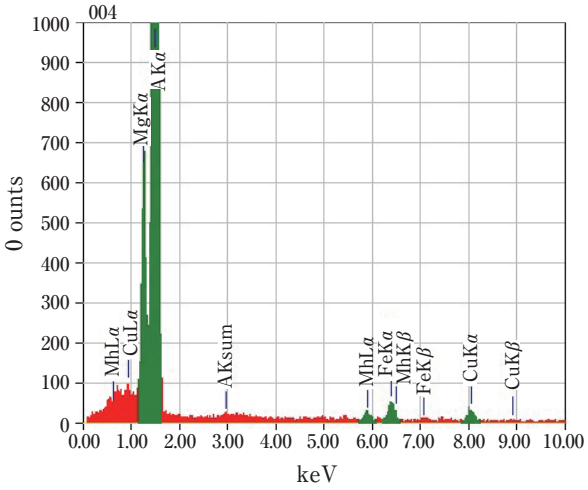

(b) Fine particle 2 (Al-Mn-Fe compound)
5082 alloy

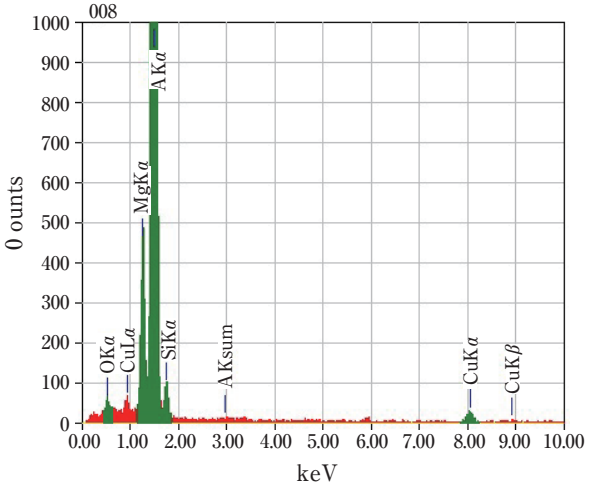

(e) Needle-like particle 2 (Mg_2Si)
5182 alloy

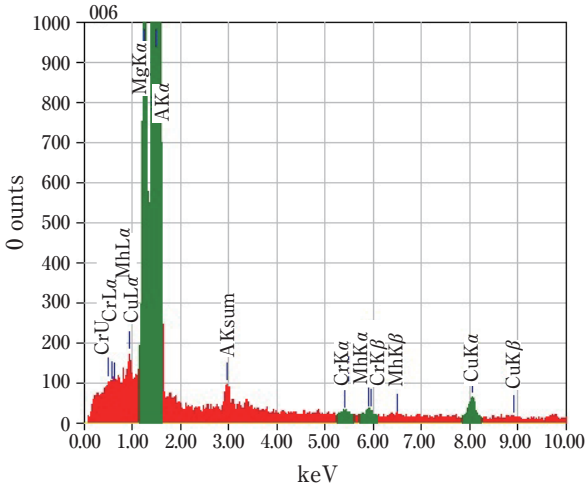

(c) Fine particle 3 (Al-Cr compound)
5082 alloy

Fig. 10 EDS analysis of the particles for 5082 and 5182 alloys in Fig.9. (a) Coarse particle 1 (Mg_2Si) in 5082 alloy, (b) Fine particle 2 (Al-Mn-Fe compound) in 5082 alloy, (c) Fine particle 3 (Al-Cr compound) in 5082 alloy, (d) Spherical particle 1 (Al-Mn-Fe compound) in 5182 alloy, (e) Needle-like particle2 (Mg_2Si) in 5182 alloy.

the 5182 alloy, including more Mn than the 5082 alloy, Al-Mn-Fe-Si compounds precipitated and coarsened during homogenization treatment. Then, Mg_2Si compounds precipitated on Al-Mn-Fe-Si compounds as precipitation sites, and grew to the needle-like shape during annealing at 618 K for 7.2 ks, whereas in the 5082 alloy, precipitation of Mn bearing compounds would be prevented during homogenization treatment; as a result, there might be less precipitation sites of Mg_2Si in the 5082 alloy. According to the precipitation of Mg_2Si, solute Mg of Al phase in the 5182 alloy would be less than that in the 5082 alloy. Thus, it is suggested that the negative strain rate dependence in the high strain rate would disappear and flow stress would increase in the 5182 alloy. Additionally, in the 5182 alloy, the particle size was lager and number of precipitates was more than the 5082 alloy, which would cause the increase of flow stress.

Fig. 10 EDS analysis of particles for 5082 and 5182 alloys in Fig. 9. (a) Coarse particle 1 (Mg_2Si) in 5082 alloy, (b) Fine particle 2 (Al-Mn-Fe compound) in 5082 alloy, (c) Fine particle 3 (Al-Cr compound) in 5082 alloy, (d) Spherical particle 1 (Al-Mn-Fe compound) in 5182 alloy, (e) Needle-like particle2 (Mg_2Si) in 5182 alloy.

4.4.3 Influence of Temperature Increase Caused by Adiabatic Heating in Impact Test

In a previous study on Al-Mg alloys, the tendency of the negative strain rate dependence was confirmed up to the strain rate of approximately 10^3 s^{-1} [26]. Additionally, it was proposed that the temperature increase caused by adiabatic heating may also affect the pinning effect of the Mg atoms in the impact test [26]. This temperature increase is expressed by the following equation [15] :

$$\Delta T = \frac{\eta}{c\rho}\int_0^{\varepsilon} \sigma d\varepsilon \tag{10}$$

where ε is the plastic strain, η is the ratio representing the transformation of the plastic work transformed into heat, and c, and ρ are the specific heat and density of the materials, respectively. The value of η was 0.9 for pure aluminum [28], and this value was also used in this study. The values of c and ρ were taken from the literature [29] and were 900 J/(kg・K) and 2660 kg/m^3, respectively. In the impact test of the 5082 alloy, the temperature increase that was calculated from the plastic work up to the strain of the maximum stress was approximately 20 K. It was surmised that this temperature increase did not affect the change in the flow stress. However, the effect of the temperature increase on the pinning effect was undeniable. In future work, it will be necessary to clarify the effect of the temperature and strain rate on the basis of the thermal activation theory of dislocation in the Al-Mg alloy.

5. Conclusions

In this study, we investigated commercial pure aluminum (1070) and commercial aluminum alloys with different Mg content amounts (5005 alloy, 5021 alloy, 5082 alloy, and 5182 alloy) and obtained their tensile properties within a wide strain rate range of 1.0×10^{-4} to 1.0×10^3 s^{-1} under room temperature. The dynamic and the impact tensile tests were conducted by using the servo-hydraulic testing machine and SHB apparatus, respectively. The 1070 exhibited the positive strain rate dependence governed by thermal activation theory of dislocation motion. On the other hand, it was found that the 5xxx series aluminum alloys exhibited mainly negative strain rate dependence and serration depending on the Mg content and the strain rate, which was caused by the PLC effect. However, the flow stress increased at high strain rate in investigated Al-Mg alloy. Therefore, the thermal activation theory became the dominant mechanism because the Mg atoms could not migrate to the dislocation at such high strain rate. As a result of using the material constitutive equation for the negative strain rate dependence, which has been proposed by Kabrian et al. [15], it was found that the flow stress may change in the dynamic strain rate range. However, by comparing the results obtained with the 5082 and the 5182 alloys, it was found that the strain rate dependence differed. It would be caused by less solute Mg of Al phase in 5182 alloy than 5082 alloy, because more Mg_2Si compounds precipitated on Mn bearing particles as precipitation sites in 5182 alloy. In addition, it was surmised that the temperature increase caused by adiabatic heating did not affect the change in the flow

stress in the investigated Al-Mg alloys.

Acknowledgments: The authors would like to thank Kinya Ogawa from the Institute of Space Dynamics (Japan) for assisting with the conduct of the dynamic and impact tensile test.

References

1) Huh, H., Ahn, K., Lim. J.H., Kim, H.W. and Park, L.J. : "Evaluation of dynamic hardening models for BCC, FCC and HCP metals at a wide range of strain rates," J. Mater. Proc. Tech., **214** (2014), 1326–1340.
2) Hopkinson, B.: "A method of measuring the pressure produced in the detonation of high explosives or by the impact of bullets," Philos. Trans. R. Soc. London A, **213** (1914), 437–456.
3) Kolsky, H.: "An investigation of the mechanical properties of materials at very high rates of loading, " Proc. Phys. Soc. Sect. B., **62** (1949), 676–700.
4) Reed, J.M. and Walter, M.E.: "Observations of serration characteristics and acoustic emission during serrated flow of an Al-Mg alloy," Mater. Sci. Eng. A, **359** (2003), 1–10.
5. Fan, G.J., Wang, G.Y., Choo, H., Liaw, P.K., Park, Y.S., Han, B.Q. and Lavernia, E.J.: "Deformation behavior of an ultrafine-grained Al–Mg alloy at different strain rates," Scr. Mater., **52** (2005), 929–933.
6) Picu, R.C., Vincze, G., Ozturk, F., Gracio, J.J., Barlat, F. and Maniatty, A.M.: "Strain rate sensitivity of the commercial aluminum alloy AA5182-O," Mater. Sci. Eng. A, **390** (2005), 334–343.
7) Coër, J., Manach, P.Y., Laurent, H.M., Oliveira, C. and Menezes, L.F.: "Piobert–Lüders plateau and Portevin–Le Chatelier effect in an Al–Mg alloy in simple shear," Mech. Res. Commun., **48** (2013), 1–7.
8) Cai, Y., Yang, S., Fu, S., Zhang, D. and Zhang, Q.: "Investigation of Portevin–Le Chatelier band strain and elastic shrinkage in Al-based alloys associated with Mg contents," J. Mater. Sci. Tech., **33** (2017), 580–586.
9) Brindley, B.J. and Worthington, P.J.: "Serrated yielding in Aluminium-3% Magnesium," Acta Metall. **17** (1969), 1357–1361.
10) Eremin, V. I.: "Effect of sample cross-section geometry and loading type on low temperature unstable plastic deformation," Scr. Metall. Mat. **25** (1991), 2215–2219.
11) Zhu, S.M. and Nie, J.F.: "Serrated flow and tensile properties of a Mg–Y–Nd alloy," Scr. Mater., **50** (2004), 51–55.
12) Garat, V., Cloue, J.-M., Poquillon, D. and Andrieu, E.: "Influence of Portevin–Le Chatelier effect on rupture mode of alloy 718 specimens," J. Nuclear Mater., **375** (2008), 95–101.
13) Wang, Z., Li, J., Yuan, B., Wu, R., Fan, J. and Wang, B.: "Serration behavior in $Pd_{77.5}Cu_6Si_{16.5}$ Alloy," Metals, **6** (2016), 191.
14) Rusinek, A. and Rodríguez-Martínez, J.A.: "Thermo-viscoplastic constitutive relation for aluminium alloys, modeling of negative strain rate sensitivity and viscous drag effects," Mater. Des., **30** (2009), 4377–4390.
15) Kabirian, F., Khan, A.S. and Pandey, A.: "Negative to positive strain rate sensitivity in 5xxx series aluminum alloys: Experiment and constitutive modeling," Int. J. Plast., **55** (2014), 232–246.
16) Huskins, E.L., Cao, B. and Ramesh, K.T.: "Strengthening mechanisms in an Al–Mg alloy," Mater. Sci. Eng. A., **527** (2010), 1292–1298.
17. Kami, T., Yamada, H. and Ogasawara, N.: "Dynamic behaviour of Al-Mg aluminum alloy at a wide range of strain rates," EPJ Web Conf. (accepted).
18) Yamada, H., Tsurudome, M., Miura, N., Horikawa, K. and Ogasawara, N.: "Ductility loss of 7075 aluminum alloys affected by interaction of hydrogen, fatigue deformation, and strain rate," Materials Science and Engineering, **A, 642** (2015), 194–203.
19) Khan, A.S. and Huang, S.: "Experimental and theoretical study of mechanical behavior of 1100 aluminum in the strain rate range 10^{-5}-10^{4} s^{-1}," Int. J. Plast., **8** (1992), 397–424.
20) Huang, S. and Khan, A.S.: "Modeling the mechanical behaviour of 1100-0 aluminum at different strain rates by the bodner-partom model," Int. J. Plast., **8** (1992), 501–517.
21. McCormigk, P.G.: "A model for the Portevin-Le Chatelier effect in substitutional alloys," Acta Metall., **20** (1972), 351–354.
22) Kubin, L.P.; and Estrin, Y.: "Evolution of dislocation densities and the critical conditions for the Portevin-Le Châtelier effect," Acta Metall. Mater., **38** (1990), 697–708.
23) Wang, C., Xu, Y. and Han, E.: "Portevin-Le Chatelier effect of LA41 magnesium alloys," Front. Mater. Sci. China, **1** (2007), 105–108.
24) Salvado, F.C., Teixeira-Dias, F., Walley, S.M., Lea, L.J. and Cardoso, J.B.: "A review on the strain rate dependency of the dynamic viscoplastic response of FCC metals," Prog. Mater. Sci., **88** (2017), 186–231.
25) Johnson, G.R. and Cook, W.H.: "A constitutive model and data for metals subjected to large strains, high strain rates, and high temperatures," Proc. 7th Inter. Sympo. Ballistics 1983, 541–547.
26) Mukai, T., Ishikawa, K. and Higashi, K.: "Strength and ductility under dynamic loading in fine- grained IN905XL aluminum alloy," Metall. Mater. Trans. A., **26A** (1995), 2521–2526.
27) The Japan Institute of Light Metals: "Structures and Properties of Aluminum," The Japan Institute of Light Metals, (1991), 221.
28) Hayashi, T., Yamaura, H. and Shigeru, O.: "Temperature measurement of metals under high velocity deformation," Proc. 20th Japan Cong. Mater. Res., (1977), 94–98.
29) Zhao, K. and Fan, R.: "The effect of pulse electric current on the mechanical properties and fracture behaviors of aluminum alloy AA5754," J. Eng. Mater. Tech., **138** (2016), 041009.

Hiroyuki Yamada
Department of Mechanical Engineering,
National Defense Academy

Tsuyoshi Kami
Graduate School of Science and Engineering,
National Defense Academy

Ryota Mori
Development Department Ⅰ,
Research and Development Division,
UACJ Corporation

Tomoyuki Kudo
Development Department Ⅰ,
Research and Development Division,
UACJ Corporation

Minemitsu Okada
No.1 Product Design Section,
Quality Assurance Department,
UACJ (Thailand) Co., Ltd.